VI Encontro de Modelagem Computacional

Instituto Politécnico da UERJ
1 a 3 de dezembro de 2003
Nova Friburgo, RJ
ISBN: 85-903068-2-8

COMPUTATIONAL MODELLING OPPORTUNITIES IN MULTI-FLUID AND FREE SURFACE FLOWS

Norberto Mangiavacchi – norberto@uerj.br
Universidade do Estado do Rio de Janeiro, Departamento de Engenharia Mecânica
Rua São Francisco Xavier, 524 – Rio de Janeiro, RJ, Brasil
Antonio Castelo Filho – castelo@icmc.usp.br
Fabricio Simeoni de Sousa – fsimeoni@icmc.usp.br
José A. Cuminato – jacumina@icmc.usp.br
Kemelli Campanharo Estacio – kemelli@icmc.usp.br
Luis G. Nonato – nonato@lcad.icmc.usp.br
Murilo F. Tomé – murilo@lcad.icmc.usp.br
Valdemir G. Ferreira – valdemir@lcad.icmc.usp.br
Universidade de São Paulo, Departamento de Ciências de Computação e Estatística
Cx.P. 668 – 13560-161 – São Carlos, SP, Brasil

Abstract. *Multi-fluid and free surface flows offer a great variety of computational modelling opportunities. In this paper, a short description of various computational modelling techniques employed by the authors is presented. Methods based on the GENSMAC front-tracking method (Tomé, M. F., McKee, S. ,1994), for 2-D and 3-D flows, for Newtonian and Non-Newtonian free-surface flows are briefly explained. The velocity field, in GENSMAC, is computed using a finite-difference scheme in an Eulerian grid, while the free-surface and the interfaces are represented by an unstructured Lagrangian grid. Surface and interface tensions are also considered and the required curvatures are approximated at the fronts by a methodology described in Castelo et al. (1999). Some applications to multi-fluid and Non-Newtonian cases are exemplified. Current developments for viscoelastic free-surface flows are sketched, and perspectives for future developments are discussed. Extensions of the GENSMAC method to deal with unstructured grids, and combining VOF or level-set strategies will also be presented.*

Keywords: *Numerical simulation, Multiphase flows, Free-surface flows, Surface tension.*

1. INTRODUCTION

Free surface and multi-phase flows are relevant to many industrial problems, such as oil, nuclear, chemical and food industry. Additionally, surface tension effects are important in applications involving small drops like in ink jet printing, coating, and paint drying.

In this work, it is described a numerical method to simulate multi-phase flows with free surfaces, considering surface and interface tension effects. The fluids are taken to be incompressible, but having different properties, like density and viscosity. All phases are considered as

a continuum, with variable properties according to the position of the interface. This approach eliminates the requirement to use explicit coupling conditions at the interface. The interface tension effects are incorporated as a source term in the momentum equation.

The numerical method was implemented in the FREEFLOW-3D simulation environment code, which uses the GENSMAC method to solve the Navier-Stokes equations. The method presented here is based on the GENSMAC method and the front-tracking methodology, having moving marking particles on the surface and the interface.

2. THE MULTI-FLUID GENSMAC METHOD

The governing equations for the incompressible flows are the Navier-Stokes equations. Considering the interface tension forces on the interface and variable properties, the momentum equation is given by

$$\frac{\partial \mathbf{u}}{\partial t} + \nabla \cdot (\mathbf{u}\mathbf{u}) = -\frac{1}{\rho}\nabla p + \frac{1}{\rho Re}\nabla \cdot \Big(\mu(\nabla \mathbf{u} + \nabla \mathbf{u}^T) + \Sigma\Big) + \frac{1}{Fr^2}\mathbf{g} - \frac{\sigma\kappa}{\rho We}\nabla H. \tag{1}$$

where $Re = \rho_0 LU/\mu_0$, $Fr = U/\sqrt{Lg}$ and $We = \rho_0 LU^2/\sigma_0$ denotes the Reynolds number, the Froude number and the Weber number, respectively. Here, L and U are the length and velocity scales, ρ_0, μ_0 and σ_0 are the reference values of density, dynamic viscosity and surface tension constants, and g denotes the gravitational constant. Furthermore, $\mathbf{u}$ denotes the velocity field, and p is the dimensionless pressure, Σ represent a viscoelastic tensor, κ is the nondimensional curvature, and $H(x, y, z, t)$, a Heaviside function defined by

$$H(x, y, z, t) = \int_{A(t)} \delta(x - x')\delta(y - y')\delta(z - z')\, da'.$$

The viscosity $\mu(q)$ can be any function representing the shear-thinning (or shear-thickening) behaviour of the fluid. In this work, we use the flollowing typical functional dependence of μ on q:

$$\mu(q) = \mu_\infty + \frac{\mu_0 - \mu_\infty}{1 + (Kq)^m}, \tag{2}$$

where μ_∞ is the infinite-shear-rate viscosity, K and m are positive constants, and the local shear rate q is given by

$$q(r, z, t) = \sqrt{2\left(\frac{\partial u}{\partial r}\right)^2 + 2\left(\frac{\partial v}{\partial z}\right)^2 + 2\left(\frac{u}{r}\right)^2 + \left(\frac{\partial u}{\partial z} + \frac{\partial v}{\partial r}\right)^2}.$$

All the fluids are taken to be incompressible, so the velocity field is divergence free, resulting in the continuity equation

$$\nabla \cdot \mathbf{u} = 0. \tag{3}$$

These equations are solved based on the GENSMAC method (Tomé, M. F., McKee, S. ,1994), in an extension of the methodology described in Santos *et al.* (2001) for two-dimensional case. It is supposed that the velocity field $\mathbf{u}(\mathbf{x}, t_0)$ is known at a given time t_0, and the boundary conditions for the velocity and pressure are given. The updated velocity field $\mathbf{u}(\mathbf{x}, t)$, at $t = t_0 + \Delta t$ is calculated using the following algorithm:

1. Let $\tilde{p}(\mathbf{x},t)$ be a pressure field which satisfies the correct pressure conditions on the free surface. This pressure field is computed according to the required boundary stress conditions.

2. The intermediate velocity field $\tilde{\mathbf{u}}(\mathbf{x},t)$ is computed by the explicitly discretized form of

$$\frac{\partial\tilde{\mathbf{u}}}{\partial t}+\nabla\cdot(\mathbf{uu})=-\frac{1}{\rho}\nabla\tilde{p}+\frac{1}{\rho Re}\nabla\cdot\Big(\mu(\nabla\mathbf{u}+\nabla\mathbf{u}^T)+\Sigma\Big)+\frac{1}{Fr^2}\mathbf{g}-\frac{\sigma\kappa}{\rho We}\nabla H \qquad (4)$$

   with $\tilde{\mathbf{u}}(\mathbf{x},t_0)$ = $\mathbf{u}(\mathbf{x},t_0)$ using the correct boundary conditions for $\mathbf{u}(\mathbf{x},t_0)$. It can be shown (Tomé, M. F., McKee, S. ,1994) that $\tilde{\mathbf{u}}(\mathbf{x},t)$ possesses the correct vorticity at time t. However, $\tilde{\mathbf{u}}(\mathbf{x},t)$ does not satisfy equation (3). Let

$$\mathbf{u}(\mathbf{x},t)=\tilde{\mathbf{u}}(\mathbf{x},t)-\frac{1}{\rho}\nabla\psi(\mathbf{x},t) \qquad (5)$$

   with

$$\nabla\cdot\frac{1}{\rho}\nabla\psi(\mathbf{x},t)=\nabla\cdot\tilde{\mathbf{u}}(\mathbf{x},t). \qquad (6)$$

   Thus, $\mathbf{u}(\mathbf{x},t)$ now satisfies equation (3) and the vorticity remains unchanged. Therefore, $\mathbf{u}(\mathbf{x},t)$ is identified as the updated velocity field at time t.

3. Solve the elliptic equation (6).

4. Compute the velocity by equation (5).

5. Compute the pressure using

$$p(\mathbf{x},t)=\tilde{p}(\mathbf{x},t)+\frac{\psi(\mathbf{x},t)}{\Delta t}$$

6. Update the positions of the marker particles.

The last step in the calculation involves moving the marker particles to their new positions. These are virtual particles whose coordinates are stored and updated at the end of each cycle by solving $d\mathbf{x}/dt=\mathbf{u}$ by Euler's method. This provides the new coordinates of every particle, allowing us to determine whether or not it moved to a new computational cell or if it left the containment region through an outlet. Using the front-tracking methodology (Unverdi, Tryggvason, 1991) only marker particles on the free surface and the interface need to be considered.

For the solution of (4), appropriate boundary conditions are applied. At solid walls null velocities are enforced. At the free surface, the boundary conditions for pressure and velocity, assuming zero viscous stress in the empty phase, are given by

$$(\mathbf{T}\cdot\mathbf{n})\cdot\mathbf{n}=p_{cap},\quad (\mathbf{T}\cdot\mathbf{n})\cdot\mathbf{m}_1=0,\quad (\mathbf{T}\cdot\mathbf{n})\cdot\mathbf{m}_2=0 \qquad (7)$$

where $\mathbf{n}$, $\mathbf{m}_1$ and $\mathbf{m}_2$ are the local normal and tangential vectors to the free surface. $\mathbf{T}$ is the viscous stress tensor and $p_{cap}=\sigma\kappa/We$ is the capillary pressure, originating from the effects of surface tension σ. Here $We=\rho LU^2/\sigma$ is the Weber number, and κ is the non-dimensional curvature. The elliptic equation (6) is solved satisfying Dirichlet boundary conditions at the free

surface and Neumann at the solid boundaries, using the conjugate gradient method. However, as the density variation across the interface is increased, more iterations are required for the convergence of the method. In these cases, we used a diagonal preconditioner to speed-up the convergence of the conjugate gradient method.

3. DISCRETIZATION

Similarly to MAC (Welch *et al.* 1965), SMAC (Amsden, Harlow, 1970) and GENSMAC (Tomé, M. F., McKee, S. ,1994) methods, the eqs. (4)–(6) are discretized by finite differences in a staggered grid. However, in this method, the fluid domain is tracked using particles only in the free surface and in the interfaces. Additionally, the nonlinear terms in the momentum equation are discretized using the high order upwind scheme VONOS (Ferreira *et al.*, 2002). Using the tracking particles, the free surface and the interface is approximated by a piecewise linear surface and represented by the "half-edge" data structure.

The flow properties are represented in a three-dimensional uniform grid, in which every cell, at each time step, is classified according to its position relative to the fluids and the rigid boundaries (eg. containers, inflow boundaries). Cells with more than half of their volume in a container are classified as BOUNDARY ($\mathbf{B}$) cells; the same criteria is used for the INFLOW ($\mathbf{I}$) cells. Any cell completely inside the fluid is classified as FULL ($\mathbf{F}$) cell, those completely outside the fluid are EMPTY ($\mathbf{E}$) cells and those on the free surface are SURFACE ($\mathbf{S}$) cells. This criteria is applied to each fluid in the simulation, and the interface cells are identified as the cells that are SURFACE ($\mathbf{S}$) for more than one fluid at the same time.

In the computation of the free surface boundary conditions, given by eq. (7) in each $\mathbf{S}$ cell, we need to have approximations for the surface normals. These are usually obtained according to the classification of the neighboring cells. For example: $\mathbf{n}_{\text{C}} = (\pm 1, 0, 0)$, $\mathbf{n}_{\text{C}} = (0, \pm 1, 0)$ or $\mathbf{n}_{\text{C}} = (0, 0, \pm 1)$ if only one neighbor is an $\mathbf{E}$ cell; $\mathbf{n}_{\text{C}} = (\frac{\pm\sqrt{2}}{2}, \pm\frac{\sqrt{2}}{2}, 0)$ if there are two neighbor $\mathbf{E}$ cells in the x and y directions, and; $\mathbf{n}_{\text{C}} = (\pm\frac{\sqrt{3}}{3}, \pm\frac{\sqrt{3}}{3}, \pm\frac{\sqrt{3}}{3})$ if there are three neighbor $\mathbf{E}$ cells in the x, y and z directions. For the implementation of the surface tension effects it is also necessary to estimate the surface curvature at the center of each surface cell, and to take into account sub-cell surface tension effects. These implementations were made and described by Sousa *et al.* (2001a, 2001b).

The interface tension effects are given by the discretization of $(\sigma\kappa'/\rho We)\nabla H$ in the faces of the interface cells if the corresponding neighboring cell is FULL for some phase. Half of the interface force is applied in these faces, and so, the interface is at most one cell thick. When the interface tension term is discretized, the forces to be applied in each direction result to be

$$F_x = \pm\frac{1}{\Delta x}\frac{\sigma\kappa'}{\rho_{i+\frac{1}{2},j,k}We}, \quad F_y = \pm\frac{1}{\Delta y}\frac{\sigma\kappa'}{\rho_{i,j+\frac{1}{2},k}We}, \quad F_z = \pm\frac{1}{\Delta z}\frac{\sigma\kappa'}{\rho_{i,j,k+\frac{1}{2}}We}$$

The sign of the forces is chosen according to the interface normal used in the computation of the curvature.

4. APPLICATIONS

The described methodology can be applied to a large variety of problems, coming from food industry, oil industry, plastic and steel industry among many others. In this section some applications involving non-Newtonian and multi-fluid cases are exemplified.

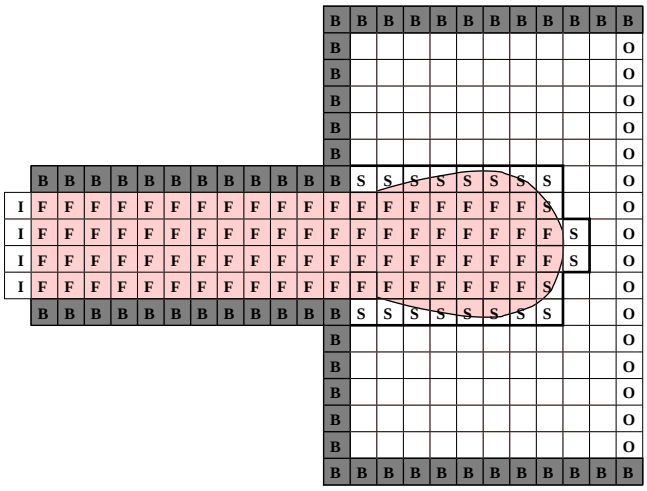

Figure 1: Domain, grid and cells.

4.1 Generalized Newtonian free surface problems: container filling and jet inpingement

Container filling and jet impingement are problems frequently encontered in the food industry. In such applications the fluid is usually very viscous, shear thinning, and can be well described by a generalized Newtonian "Powel Law" model, Eq. (2). Figure 2 shows results of numerical simulations of container filling comparing the behavior of Newtonian jet with generalized Newtonian jets. The data for these simulation were: fluid velocity at nozzle: U = 1.0 ms^{-1}, nozzle diameter: D = 10 mm. The fluid was modelled by the Cross model: ν_∞ = 0.001 m^{2}s^{-1}, ν_0 = 0.01 m^{2}s^{-1}, K = 0.3, m = 1.0. $Re = UD/\nu_0$ = 1.0 $1/Fr^2$ = 0.01, $L1$ = 6 cm, $L2$ = 5 cm and H = 7 cm, $\delta r = \delta z = 1$ mm was employed, giving 60 $\times$ 80 cells within the mesh.

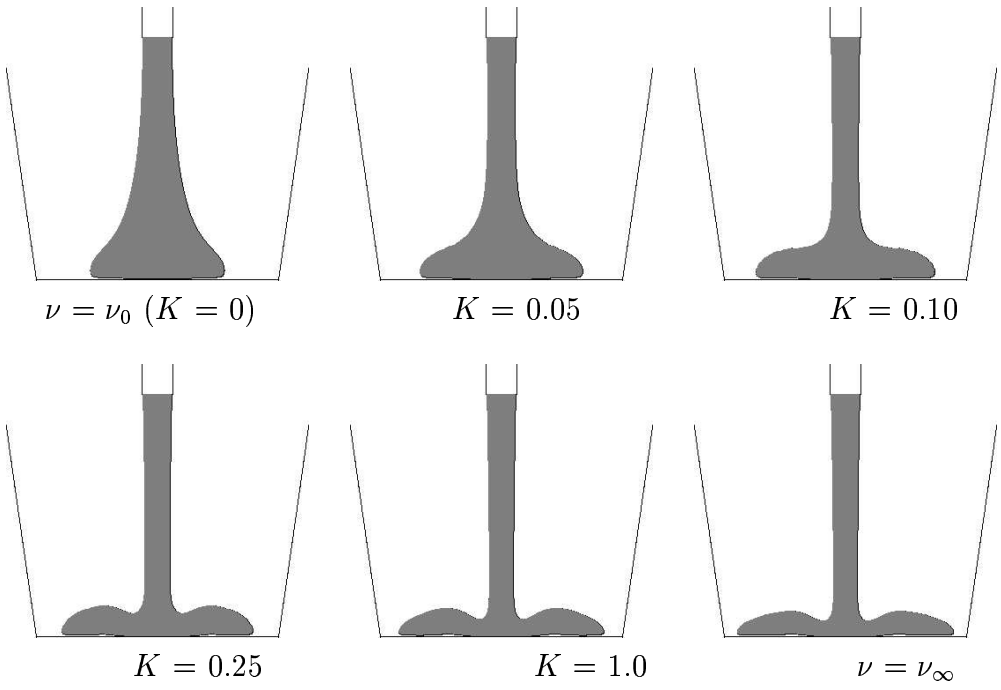

Figure 2: Numerical simulation of cavity filling for various values of K at time $t = 40.0$.

4.2 Surface tension effects: drop formation and bubble burst

Drop and bubbles occour in many technological applications such as ink jet printers, gas-liquid exchangers, and many manufacturing processes. In this class of problems, surface tension effects are important, and must be modelled accurately. In this section we present examples of simulations of axisymmetric sessile and pendant drops. These are useful for validation of the method because, for these stationary cases, it is possible to find assymptotic solutions to compare.

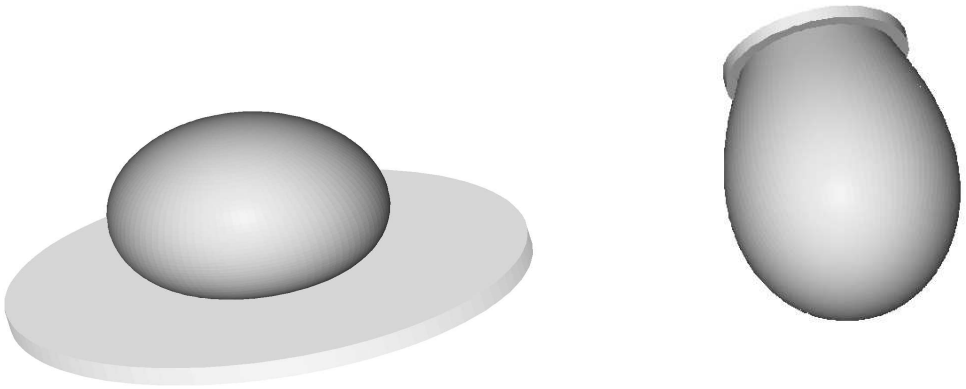

(a) Sessile drop: $L^2\rho g/\sigma = 1.962$, $\delta x = \delta y = 0.04L$, and $\delta x = \delta y = 0.067L$

(b) Pendant drop: $L^2\rho g/\sigma = 0.1962$, and $\delta x = \delta y = 0.05L$

Figure 3: Numerical solution for axisymmetric sessile (left) and axisymmetric pendant drop (rigth).

The results presented in Fig 3 are obtained from axisymmetric simulations, that were rendered in 3D to help in the visualization.

The motion of a free surface after a bubble has burst-through has also been used as a benchmark for comparison of numerical methods by various authors (see e.g. Sussman, Smereka, Osher, 1994). In figure 4 we present results from calculations with $Re = \frac{UD}{\nu} = 118.5$, $Fr = 3.65$, and $We = 2$, where D is the bubble diameter. This corresponds approximately to a 4mm bubble bursting on the water surface.

Figure 4: Bursting bubble simulation at times $t = 0,\ 0.08,\ 0.16,\ 0.24,\ 0.32,$ and 0.64, 3D view.

Computations were performed using the domain $\Omega = \{(r, z) :\ 0 \leq r \leq 1.5$ and $0 \leq z \leq 6\}$, discretized using a grid of 60×240 uniform cells, to allow for the height to which the

satellite drops travel. The simulation begins ($t = 0$) after the bubble has just started to burst open. The simulation shows initially how the rim of the crater is pulled outwards by surface tension. The last frame in the sequence shows the development of a jet from the bottom of the crater that finally breaks up due to capillary instabilities, emitting satellite drops.

4.3 Multifluid flows: bubble flows

Rising bubbles are classical examples to validate multi-phase flows simulations. Bubbles with lower density than the surrounding fluid tend to rise, due to the hydrostatic effects that increase the pressure towards the bottom of the domain.

This example shows the simulation of the three-phase flow of two bubbles with different properties and diameters, raising in a third phase with the larger density.

The bubbles rise due to buoyancy forces. The nondimensional paremeters are: $Re = 55.75$, $Fr = 1$, $We = 4.6$. For the continous phase, $\rho_f = 880\ kg/m^3$ and $\mu_f = 0.0125\ Ns/m^2$. For the larger bubble, $D_1 = 4\ mm$, $\rho_1 = 88\ kg/m^3$ and $\mu_1 = 0.00125\ Ns/m^2$, with $Eo_1 = 4.6$. Finally, for the smaller bubble, $D_2 = 2\ mm$, $\rho_2 = 176\ kg/m^3$ and $\mu_2 = 0.0025\ Ns/m^2$, with $Eo_2 = 1.15$. The surface tension coefficient for all interfaces is $\sigma_I = 0.03\ N/m$. The lenghts and velocities were nondimensionalized using $D_1 = 4\ mm$ and $U = \sqrt{gD_1}$, respectively. The grid used in this example was $32 \times 32 \times 64$ cells.

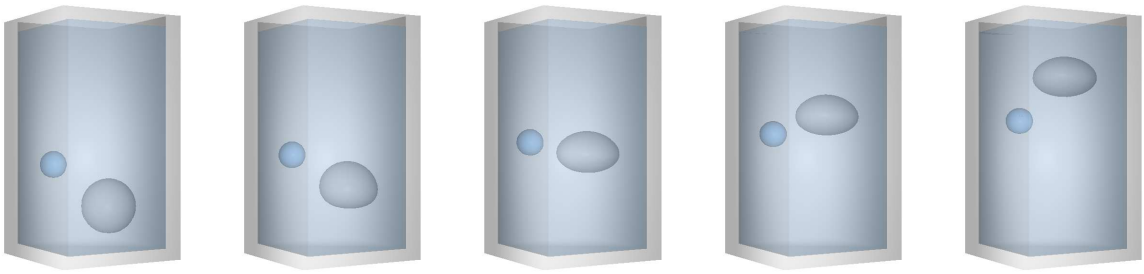

(a) $t = 0\ s$ (b) $t = 0.02\ s$ (c) $t = 0.04\ s$ (d) $t = 0.06\ s$ (e) $t = 0.08\ s$

Figure 5: Raising of two bubbles with different properties.

Figure 5 shows the time evolution of the flow. It can be seen that the larger bubble undergoes a larger deformation than the smaller bubble, due to its larger Eötvös number. It can also be oberved a small deflection in the trajectory of the smaller bubble, which is due to the interaction with the larger bubble as it passes by.

4.4 Bubble coalescence

Another classical example of multi-phase flows is the coalescence of two bubbles in a continuous phase. This problem was simulated with good results, as can be seen below. The bubbles diameter is $D = 2.6\ mm$, the velocity is nondimensionalized by $U = \sqrt{gD} = 0.15\ m/s$, the interface tension coefficient is $\sigma = 5.8 \times 10^{-4}\ N/m$, and the dimensionless constants $Re = 30$ and $Eo = 100$ are the Reynolds and Eötvös numbers, respectively. For the continuous phase, $\rho_f = 880\ kg/m^3$, $\mu_f = 0.0125 Ns/m^2$, and for the drops, $\rho_d = 440\ kg/m^3$, $\mu_d = 0.00625 Ns/m^2$. Figure 6 (left) shows the transient solution of the interface, with the coalescence of both drops, starting from the drops initialy in-line.

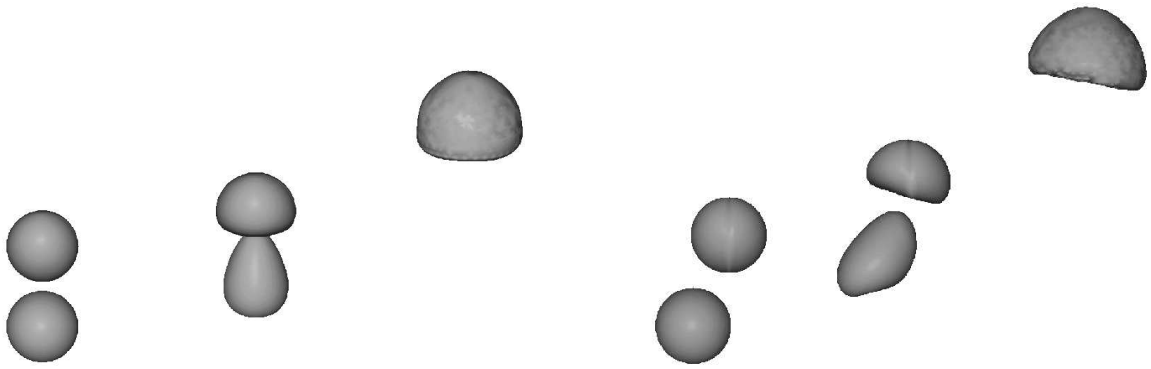

Figure 6: left: Transient solution of the bubble coalescence in a continuous phase, with in-line bubbles, for $t = 0.0\ s$, $t = 0.03\ s$, $t = 0.06\ s$, $t = 0.09\ s$, $t = 0.12\ s$ and $t = 0.15\ s$.right: Transient solution of the bubble coalescence in a continuous phase, the bubbles are not in-line, for $t = 0.0\ s$, $t = 0.03\ s$, $t = 0.06\ s$, $t = 0.09\ s$, $t = 0.12\ s$ and $t = 0.15\ s$.

The same flow parameters were utilized to simulate the rise of two bubbles that are initially not aligned. Figure 6 (right) shows the 3D rendering of the transient solution, in which the bottom bubble seeks the top bubble until the coalescence, due the lower pressure field at the bottom of the top bubble. These results are in very good agreement when compared with the numerical results obtained by Li Chen & Yuguo Li (1998) and the experimental results by Narayanan et. al. (1974).

4.4 Unstructured grids: plastic injection

The flow of a fluid characterized by high viscosity in a narrow gap is a problem typically found in processes of injection molding. In this case, the flow can be described by few suitable simplifications in the three dimensional conservation equations, in a formulation known as Hele-Shaw approach (Bretas, M. A. D'Avila, 2000) Such simplifications can be obtained using a number of assumptions regarding the injected polymer and the geometry of the mold, together with the integration and the coupling of the momentum and continuity equations.

In this section we present results obtained with an extension of the above technique for the simulation of the molding injection process of polymers using unstructured meshes. This technique considers important aspects to guarantee the quality of the part, such as the transference of heat by the walls and the points of insertion of the mold, and the influence of the temperature in the fluidity of the polymer. The implemented numerical method uses the topological data structure SHE – Singular Handle Edge (Nonato, Castelo, Oliveira, 2002), capable to deal with boundary conditions and singularities, aspects commonly found in numerical simulation of fluid flow.

The governing equations are resolved using an unstructured mesh, generated by Delaunay triangulation (Shewchuk, 1999) and the discretization method is based on the finite volume formulation (Maliska, 1995). In this section we present some results obtained using an unstructured triangular mesh with 905 elements. This quantity of elements may be considered small, but provides better visualization of the results.

In this test problem, we use prescribed pressure and temperature boundary conditions at the mold inlet. The inlet temperature T is initialized with $373\ K$, the wall temperature T_w, with $298\ K$, and the pressure p, with $10^7\ N/m^2$ as described before. The material properties

are specific heat $c_p = 1900\ J/kgK$, density $\rho = 10^3\ kg/m^3$ and thermal conductivity $k = 10^{-1}\ W/mK$, which are typical of polypropylene. The dimensions of the mold are thickness = $1.25\ 10^{-3}\ m$, width = $10^{-1}\ m$ and length = $10^{-1}\ m$.

Figures 7 and 8 show the velocity vector and the temperature fields, respectively, at three stages: right after the flow had started, at $t = 0.39s$; in a intermediate time, $t = 4.47s$; and at its end, when $t = 16.07s$.

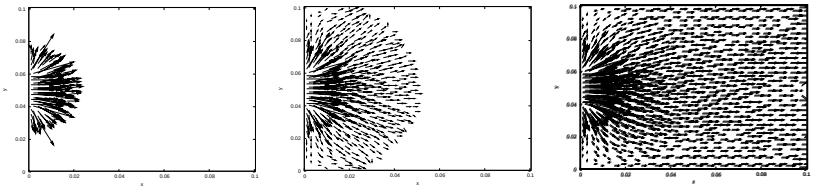

Figure 7: Velocity vectors obtained after the calculations for the pressure distribuition

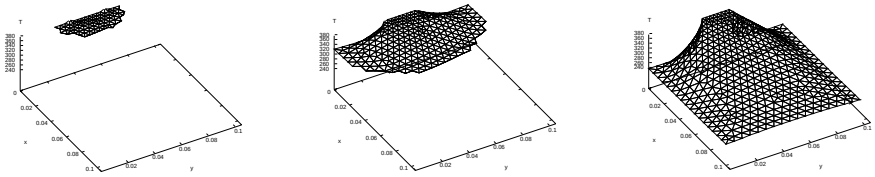

Figure 8: Three stages of the energy equation solution

Notice the appearance of two regions next to the injection area with temperatures exceeding the injection temperature (figure 8(a)). This fact is explained by the viscous dissipation, caused by the high values of the velocity at these regions and it is a very important effect to consider in injection molding processes. The prediction and control of this effect are essential to guarantee the final quality of the part, in order to produce adequate surface finish, dimension stability and mechanical properties.

5. CONCLUSIONS

In this work, it was described a method to simulate multi-phase flows with surface tension, where the fluids are taken to be incompressible. This method was based on the GENSMAC method (Tomé, M. F., McKee, S. ,1994), using finite difference scheme to discretize the governing equations, as was done in in Santos *et al.* (2001). Surface and interface tensions are considered, and the required curvature on the interface is computed by a technique of surface approximation (Castelo *et al.*, 1999)(Sousa *et al.*, 2001a, 2001b). The numerical results are in very good agreement with known analytical solutions of simple problems, like equilibrium bubble and the oscillation of a drop. Other numerical results show the robustness of the code, like rising drops and bubble coalescence. These results are comparable with numerical results obtained in Esmaeeli & Tryggvason, G. (1998, 1999), and Li Chen & Yuguo Li (1998). The extension of the method for Hele-Show problems using unstructured grids is shown.

Acknowledgements

We gratefully acknowledge support given by FAPESP (grant 00/03385-0) and CNPq (grants 460473/2001-8 and 302633/2003-0).

REFERENCES

Amsden, A. A., Harlow, F. H. (1970). “The SMAC Method: a Numerical Technique for Calculating Imcompressible Fluid Flows, Los Alamos Scientific Laboratory, Report LA-4370.

Brackbill, J. U., Kothe, D. B., Zemach, C. (1992). “A continuum method for modeling surface tension”, *Journal of Computational Physics*, 100:335–354.

Bretas, R. E. S., D’Avila, M. A.; “Reologia de Polmeros Fundidos”. Editora da UFSCar. So Carlos: 2000. 196p.

Castelo, A., Mangiavacchi, N. Cuminato, J. A., Fortuna, A. O., Oliveira, J. Tomé, M. F., McKee, S. (1999). “Surface Tension Implementation for GENSMAC2D Code”, COBEM’99, CD-ROM.

Chen, Li & Yuguo, Li (1998). “A numerical method for two-phase flow with an interface”, *Environmental Modelling & Software*, 13:247–255.

Esmaeeli, A., Tryggvason, G. (1998). “Direct numerical simulations of bubbly flows. Part 1. Low Reynolds number arrays”. *J. Fluid Mech.*, 377:313–345.

Esmaeeli, A., Tryggvason, G. (1999). “Direct numerical simulations of bubbly flows. Part 2. Moderate Reynolds number arrays”. *J. Fluid Mech.*, 385:325–358.

Ferreira, V. G., Tomé, M. F., Mangiavacchi, N., Castelo, A., Cuminato, J. A., Fortuna, A. O. (2002).“High Order Upwinding and the Hydraulic Jump”, *International Journal for Numerical Methods in Fluids*, 39:549–583.

Maliska, C. R.; “Transferncia de Calor e Mecnica dos Fluidos Computacional - Fundamentos e Coordenadas Generalizadas”, LTC - Livros Tcnicos e Cientficos. Rio de Janeiro: 1995. 424p.

Mangiavacchi, N., Castelo, A., Cuminato, J. A., Fortuna, A. O., Tomé, M. F., Nonato, L. G., McKee, S. (2000). “Numerical Simulation of Surface Tension Dominated Axisymmetric Free Surface Flows”, ENCIT, CD-ROM.

Narayanam, S., Groossens, H. J., Kossen, N. W. F. (1974). “Coalescence of two bubbles rising in line at low Reynolds number”. *Chem. Eng. Sci.*, 29:2071–2082.

Nonato, L. G., Castelo F°, A., Oliveira, M. C. F.; A Topological Approach for Handling Insertion and Removal of Triangles into Two-Dimensional Unstructured Meshes. *Submitted article*, (2002).

Santos, F. L. P., Mangiavacchi, N., Castelo, A., Tomé, M. F., Ferreira, V. G., Cuminato, J. A. (2001) “Numerical Simulation of Multi-phase Flows Using the FreeFlow-2D System”, COBEM’2001, CD-ROM.

Shewchuk, J. R.; Lecture Notes on Delaunay Mesh Generation. Available in: http://citeseer.nj.nec.com/shewchuk99lecture.html, (1999).

Sousa, F. S., Mangiavacchi, N., Castelo, A., Nonato, L. G., Tomé, M. F., Cuminato, J. A. (2001). “Simulation of 3D Free-surface Flows with Surface Tension”, COBEM’2001, CD-ROM.

Sousa, F. S., Mangiavacchi, N., Castelo, A., Nonato, L. G., Tomé, M. F., Cuminato, J. A.(2001). “A mass conserving filter for the simulation of 3D free surface flows with surface tension”, CILAMCE’2001, CD-ROM.

Sussman, M., Smereka, P., Osher, S. (1994). “A level set approach for computing solutions do incompressible two-phase flow”, *J. Comp. Phys.*, 114:146–159.

Tomé, M. F., McKee, S. (1994). “GENSMAC: A Computatinal Marker-and-Cell Method for Free Surface Flows in General Domains”. *Journal of Computational Physics*, 110(1):171–189.

Unverdi, S. O., Tryggvason, G. (1991). “A Front-Tracking Method for Viscous Incompressible Multi-Fluid Flows”. *Journal of Comp. Physics*, 100:25–27.

Welch, J. R., Harlow, F. H., Shannon, J. P., Daly, B. J. (1965). “The MAC Method”, Los Alamos Scientific Laboratory, Report LA-3425.